Centralized Control Architecture for Coordination of Distributed Renewable Generation and Energy Storage in Islanded AC Microgrids

Aldana, Nelson Leonardo Diaz; Hernández, Adriana Carolina Luna; Quintero, Juan Carlos Vasquez; Guerrero, Josep M.

Published in:
I E E E Transactions on Power Electronics

DOI (link to publication from Publisher):
10.1109/TPEL.2016.2606653

Publication date:
2017

Document Version
Early version, also known as pre-print

Centralized Control Architecture for Coordination of Distributed Renewable Generation and Energy Storage in Islanded AC Microgrids

Nelson L. Díaz, *Student Member, IEEE,* Adriana C. Luna, *Student Member, IEEE,* Juan C. Vasquez, *Senior, IEEE,* and Josep M. Guerrero *Fellow, IEEE,*

***Abstract*—The coordinated operation of distributed energy resources such as storage and generation units and also loads is required for the reliable operation of an islanded microgrid. Since in islanded microgrids the storage units are commonly responsible for regulating the voltage amplitude and frequency in the local power system, the coordination should consider safe operating limits for the stored energy, which prevents fast degradation or damage to the storage units. This paper proposes a centralized control architecture, applicable for local area power systems such as a small-scale microgrid. The centralized architecture is based on three supervisory control tasks which consider: active power curtailment of generation for avoiding overcharge of the storage units, load shedding actions for preventing deep discharge of the storage units, and equalization of the state of charge among distributed storage systems for avoiding uneven degradation. The proposed equalization method has proved to be effective for equalizing the state of charge of distributed energy storage systems and for ensuring uniform charge/discharge ratios regardless of differences in the capacity of the storage units. Additionally, the strategy is complemented with an optimal scheduling of load connection, which minimizes the connection and disconnection cycles of the loads within a time horizon of 24 hours. The proposed architecture is verified experimentally in a lab-scale prototype of a microgrid, which has real communication between the microgrid and the central controller.**

***Index Terms*—Centralized architecture, Distributed Storage and Generation, Energy Storage Equalization, Power Curtailment.**

I. Introduction

THE current trend in the integration of renewable energy sources (RESs) such as photovoltaic (PV) and wind turbine (WT) generators has imposed additional challenges in the operation of microgrids. Due to the unpredictable behaviour of the RESs, the microgrid is complemented with energy storage systems (ESSs) which help to keep the power balance of the system while satisfying the local power requirements and reducing the dependence on the utility grid [1]. A microgrid can become completely independent from the main grid and operates in islanded mode when all the distributed units (RESs, ESSs and loads) are coordinated properly. Because of that, complex microgrid management systems and coordinated control strategies are required for ensuring reliable operation of the islanded power grid [2], [3].

The use of ESSs imposes additional challenges in the management of the microgrid such as strategies that properly limit the state of charge (SoC) of the ESSs within a safe operating window (20 % to 90 %) [4]. In this sense, specific supervisory tasks such as: active power curtailment of generated energy for avoiding overcharge, and load shedding for avoiding deep discharge of the ESSs, have to be defined within the control architecture of the microgrid [2], [5]. The aforementioned considerations are particularly important for ESSs based on batteries, which are the most used in islanded applications due to the good commitment between energy density, deep-cycle life and cost [6].

Currently, distributed ESSs are preferred rather than aggregated ESSs. This fact allows a flexible and optimal integration of different kinds of RESs [7]. For a microgrid with distributed ESSs, it is recommended the equalization of the SoC between distributed storage units. The main aim of the SoC equalization is avoiding uneven degradation of the storage units caused by unequal discharge/charge cycles, resulting in overcharge or deep discharge in some of the storage units. Several strategies for SoC equalization have been widely applied for cells with similar capacity in battery strings [8], [9]. Likewise, SoC equalization methods have been broadly applied for distributed ESSs in microgrids such as in [10]–[14], where the amount of power contribution of each ESS is adaptively adjusted based on the SoC values. In this way, the ESS with the largest SoC will contribute with more power (absorbing or supplying) than the others ESSs for achieving the equalization. However, none of the aforementioned approaches have proved to be effective for the equalization of the SoCs in distributed ESSs with different capacities because they do not consider the relation between power sharing and the capacities of the ESSs.

This paper presents an alternative and effective approach for the equalization of the SoCs, even between ESSs with different capacities. The proposed equalization strategy adjusts the rate of change of the SoCs for achieving the equalization of the SOCs within specific periods. Additionally, the equalization strategy allows a proportional power sharing among distributed ESSs in accordance to their respective capacity, by ensuring equal discharge/charge rates and cycles. Compared to preliminary simulations presented in [15], this paper provides experimental validation of the proposed approach under different operational conditions. Also, this

N. L. Díaz is with the Department of Energy Technology, Aalborg University, Aalborg 9220, Denmark; and also with the Engineering Faculty, Universidad Distrital F.J.C., Bogotá 110231, Colombia (e-mail: nda@et.aau.dk; nldiaza@udistrital.edu.co).

A. C. Luna, J. C. Vasquez, and J. M.Guerrero are with the Department of Energy Technology, Aalborg University, 9220 Aalborg East, Denmark (e-mail:acl@et.aau.dk; juq@et.aau.dk; joz@et.aau.dk).

paper considers detailed analysis for proper selection of the equalization and power sharing parameters in accordance to stability considerations, power constraints and practical issues. Moreover, the equalization strategy in [15], by itself, lacks of a control architecture for allowing an appropriate interaction of the distributed ESSs with other distributed energy resources and loads in an islanded microgrid. This paper proposes a suitable coordination architecture by considering the limited storage capacity of the ESSs and integrating the equalization function.

In this sense, several control architectures have been proposed for a coordinated operation of distributed energy resources in microgrids [3], [5], [13], [16]–[27]. Some authors have pointed out the advantages of fully distributed architectures without additional communication links such as: high modularity, expandability and reliable operation [3], [5], [16]–[19]. Distributed approaches are preferred in wide area applications where communication links are not always suitable [9]. Those strategies require perturbations and deviations in the nominal operation point of the power line, even in steady state. Also, failures in single units may cause unexpected changes in the operation of the whole microgrid. On the other hand, centralized strategies based on networked control structures rely on a centralized control with a global perception of the whole microgrid by means of dedicated communication channels, which enhance the stability of the microgrid [20]–[24], [26], [27]. Additionally, networked-based control strategies offer an easy deployment of additional functions in the management systems such as voltage and frequency restoration, reactive power support, optimized operation and definition of simple supervisory actions for discrete events [13], [25]–[28]. The main drawback in the use of dedicated communication channels is that single point of failures may cause loss of the coordination of the microgrid [3]. Nevertheless, a local area network (LAN) based on wired or even wireless communication has proved to be reliable enough for small-scale microgrid applications such as small buildings, households, research laboratories, etc. [29], [30].

This paper proposes a centralized coordination architecture for a small-scale islanded microgrid. The main feature of the proposed coordination architecture is the definition of simple supervisory stages, for performing specific tasks related to: limiting the energy generation from RESs, in order to avoid overcharge of the ESSs; disconnecting the load, for avoiding deep discharge of the ESSs; and including equalization function of the SoCs among distributed ESSs with different capacities, looking for a proportional power sharing and equal discharge/charge profiles. In fact, the equalization of the discharge/charge profiles permits the management of the distributed ESSs as an aggregated one, which facilitates the definition of simpler coordinated actions with the other distributed resources in the microgrid. This feature is achieved, since the threshold values of charge and discharge are reached at the same time in all the distributed storage units. Experimental results show that the proposed coordination strategy ensures reliable operation of the local area power system while keeping a safe SoC window for the operation of the distributed ESSs based on batteries [4].

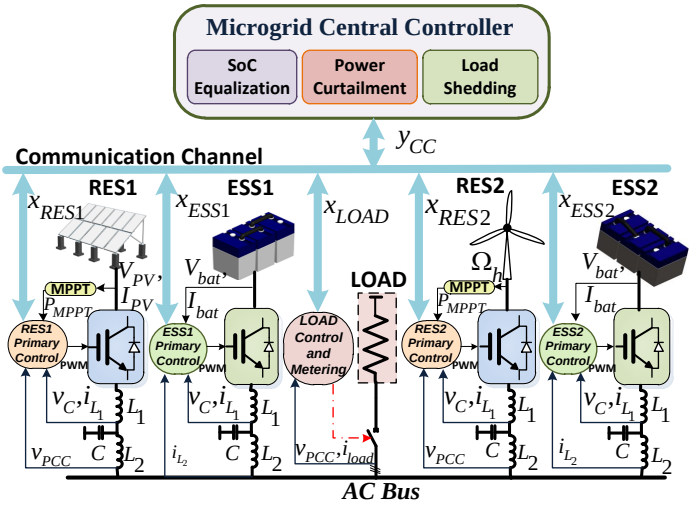

Fig. 1: Islanded AC microgrid configuration.

Apart from that, preliminary experimental results of the load shedding profile show that several disconnection cycles of the load may appear, which do not allow a continuous supply of energy to the load. This fact is particularly critical for many appliances that need to be energized for a minimum continuous time to get the job done (for instance, dishwashers or laundry machines in household microgrids). In order to overcome this problem, the proposed approach is complemented with an optimal scheduling for determining the times of load connection based on a 24-hour-ahead forecasting of generation and consumption. The proposed load scheduling minimizes the disconnections of the load and ensures the maximum time for continuous load supply with a horizon of one day. Nevertheless, the load shedding function continues operating in order to ensure safe operating limits for the ESSs by regarding possible mismatches between forecast and real operation.

Section II presents general characteristics of an islanded microgrid considered as study case, section III introduces the centralized control strategy architecture. Section IV defines the parameters and the main characteristics of the experimental microgrid. Finally, section V shows partial results without the optimized load disconnection, introduces the definition of the optimization problem and presents final results. The proposed architecture is validated in an experimental microgrid setup where a real wired communication system is used between the central controller and the distributed energy resources.

II. Small-scale Microgrid

The small-scale microgrid selected as study case is composed of hybrid PV-WT generation units, distributed ESSs based on batteries, an aggregated load and a microgrid central controller (MGCC) which is communicated with the distributed resources by means of a full-duplex communication channel as shown in Fig. 1.

The microgrid is able to operate almost autonomously by means of a multi-master slave configuration [25]. Here, the ESSs are the master units who share the responsibility of forming the common bus voltage by defining its amplitude

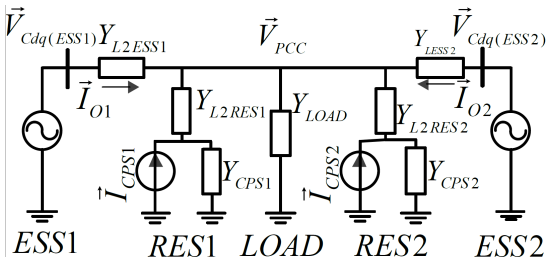

Fig. 2: Topological circuit operation of the microgrid.

and frequency, while ensuring the power balance in the islanded microgrid. The ESSs will be charged or discharged based on the unbalance between generation and consumption. Meanwhile, RESs are slave units that behave as power sources operating in current control mode (CCM) [23]. The primary controllers of the ESSs and RESs have been designed with a fast dynamic response compared with the slow dynamic required for charging and discharging the ESSs. Therefore, the master units (ESSs) can be represented with a voltage source in series with an output admittance, and the grid-following units (slaves) are represented with a current source in parallel with an admittance as shown in Fig. 2 [31].

The power balance is shared between distributed ESSs by means of conventional $P-\omega$ droop control loops. This fact allows an effective power sharing without any communication between distributed ESSs [32]. Therefore, the frequency at the common ac bus is established by the following equation,

$$\omega = \omega^* - K_p \cdot P_{Bati} \tag{1}$$

where, K_p is the droop coefficient, ω is the angular frequency at the common bus, ω^* is the reference of the angular frequency and P_{Bati} is the active power at each i-th ESS unit $(i = [1, 2])$.

On top of that, a microgrid central controller (MGCC) operates as a supervisory entity responsible for coordinating the control actions among distributed units.

III. Microgrid Central Controller - MGCC

The MGCC is responsible for performing three specific tasks oriented to ensure safe operational conditions for the ESSs based on batteries. The tasks of MGCC are: SoC equalization for avoiding uneven degradation of distributed ESSs, active power curtailment of the energy generation from RESs, which avoids overcharge of the ESSs, and load-shedding for preventing over-discharge of the ESSs based on batteries.

A. SoC Equalization for distributed ESSs

The equalization of the SoC is based on the fact that the rate of change of the SoC for the i-th ESS $(m_{SoCi} = \Delta SoC_{Bati}/\Delta t)$ is directly proportional to the battery power $(P_{Bati} \propto m_{SoCi})$. Therefore, by adjusting m_{SoCi}, and consequently the battery power, it is possible to achieve the equalization of the SoC as shown in Fig. 3.

This behaviour can be achieved by weighting the droop coefficient (K_p) in equation (1) by a factor α_i in each ESS unit. Therefore, equation (1) can be modified as follows

$$\omega = \omega^* - K_p \cdot \alpha_i \cdot P_{Bati} \tag{2}$$

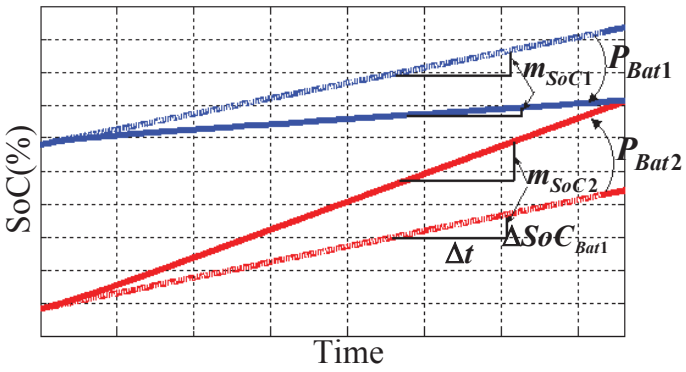

Fig. 3: Expected behaviour for the equalization of SoCs.

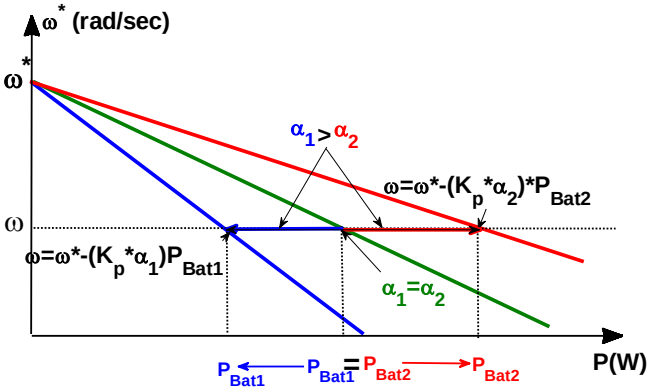

Fig. 4: Droop adjustment.

In Fig.4 is possible to see that $|P_{Bat2}| > |P_{Bat1}|$ by making $(\alpha 1 > \alpha 2)$. Also, it is possible to see from Figs. 4 and 3 that the relationship between m_{SoCi} and α_i is inversely proportional. Therefore, the problem of equalizing the SoC between distributed ESSs is reduced to determine the proper value of each α_i.

First of all, the SoC at each ESS can be estimated by ampere-hour (Ah) counting method

$$SoC(\Delta t)_{Bati} = SoC(0)_{Bati} - \int_0^{\Delta t} \eta_{Bati} \frac{I_{Bati}(\tau)}{C_{Bati}} d\tau \tag{3}$$

where, $SoC(0)_{Bati}$ is the initial SoC, C_{Bati} is the capacity in $(A \cdot h)$, η_{Bati} is the charging/discharging efficiency, and $I_{Bati}(\tau)$ is the instantaneous current at each battery array. By assuming a constant current charge, the power at each battery array can be approximated as

$$P_{Bati} \approx V_{Bati} * I_{Bati} \tag{4}$$

where (V_{Bati}) is the voltage of the battery array in each ESS. Then, from (3) and (4) is possible to obtain

$$P_{Bati} \approx -\frac{\Delta SoC_{Bati}}{\Delta t}\left(\frac{V_{Bati}C_{Bati}}{\eta_{Bati}}\right) \approx -m_{SoCi}K_{Bati} \tag{5}$$

where, K_{Bati} is a variable that contains the information about the main parameter of each battery array.

In general, for n distributed generators and storage units integrated into the microgrid, it is easy to derive the power balance equation as:

$$\sum_{i=1}^{n} P_{Bati} + \sum_{i=1}^{n} P_{RESi} - P_{load} = 0 \tag{6}$$

where P_{load} is the aggregated load consumption, and P_{RESi} is the power supplied by each RES. Combining (5) and (6):

$$\sum_{i=1}^{n}(-m_{SoCi}K_{Bati}) + \sum_{i=1}^{n}(P_{RESi} - P_{load}) = 0 \tag{7}$$

Also, under constant current charge, the behaviour of the SoC in a period (Δt) can be approximated by the straight-line equation:

$$SoC(\Delta t)_{Bati} = SoC(0)_{Bati} + m_{SoCi}\Delta t \tag{8}$$

where, $SoC(0)_{Bati}$ is the initial value and $SoC(\Delta t)_{Bati}$ is the value after Δt. For ensuring SoC equalization in a period Δt, it is required that the final value is the same for all the ESSs ($SoC(\Delta t)_{Bat(i-1)} = SoC(\Delta t)_{Bati} = SoC(\Delta t)_{Bat(i+1)}$). Then:

$$\begin{aligned}
&SoC(0)_{Bat1} + m_{SoC1}\Delta t = SoC(0)_{Bat(2)} + m_{SoC(2)}\Delta t;\\
&SoC(0)_{Bat2} + m_{SoC2}\Delta t = SoC(0)_{Bat(3)} + m_{SoC(3)}\Delta t;\\
&\vdots\\
&SoC(0)_{Bat(n-1)} + m_{SoC(n-1)}\Delta t\\
&\qquad = SoC(0)_{Bat(n)} + m_{SoC(n)}\Delta t;
\end{aligned} \tag{9}$$

At this point, it is possible to solve the linear system composed of equations (7) and (9) in order to obtain the different values of m_{SoCi} for all ESSs. Afterwards, the weighting factor α_i in (2) can be obtained for each ESS droop control loop by taking into account that:

$$\alpha_1 \cdot P_{Bat1} = \alpha_2 \cdot P_{Bat2} = \alpha_i \cdot P_{Bati} \tag{10}$$

where,

$$\begin{aligned}
\alpha_1 \cdot m_{SoC1}K_{Bat1} &= \alpha_2 \cdot m_{SoC2}K_{Bat2}\\
&= \alpha_i \cdot m_{SoCi}K_{Bati}
\end{aligned} \tag{11}$$

In order to achieve appropriate dynamic response and ensure the stability in the operation of the microgrid, the droop coefficient (K_p) should be limited to a nominal value as explained in [31], [33]. Because of that, the maximum value of the weighting factors should be 1, when K_p is set to its nominal value. Therefore, it is important to assign the maximum value of the weighting factor in accordance to the following criteria:

1) The charge or discharge of the ESSs: First, it is necessary to determine if the batteries are being charged ($sign(P_{Bati}) = 1$) or discharged ($sign(P_{Bati}) = -1$). Under the discharge process, for balancing the SoC, the ESS with the highest SoC should supply more power to the microgrid than the others. On the contrary, when the ESSs are being charged, the ESS with the smallest SoC should get more energy from the microgrid than the others.

2) The state of charge of the ESSs: When the ESSs are being charged, the ESS with the smallest SoC should get more energy from the microgrid than the others. Then, the largest weight is assigned to the ESS with the biggest value of SoC (see equation (10)). On the contrary, when the ESSs are being discharged the ESS with the highest SoC should supply more power to the microgrid than the others. Then, the largest weight is assigned to the ESS with the smallest value of SoC.

The maximum weight is defined by (K_{min}/K_{max}), where K_{min} and K_{max} are the minimum and maximum values of the parameter defined in (5). In this way, it is ensured that the droop coefficient ($\alpha \cdot K_p$) will never be greater than its nominal value. The other values of the weighting factor are obtained from equation (11).

3) Operation out of the equalization time: Since the equalization will be applied only when there are differences in the SoC and during a specified period, it is required to define how the weighting factor will be established during periods of no equalization. This is an important fact that has not been considered previously by other strategies for SoC equalization, specially for the operation of distributed ESSs with different capacities. Once the equalization has been achieved, an equal charge/discharge rate is expected for all the ESSs in order to unify the profiles of the SoCs, this is ($m_{SoCi-1} = m_{SoCi} = m_{SoCi+1}$). Due to differences at the capacities of the ESSs, the largest value of the weighting factor will be assigned to the ESS with the smallest capacity ($\alpha_i = 1$). In this way, the ESSs with the smallest capacity will contribute with less power in the power sharing defined by droop control loops. Meanwhile, the others ESS units will get a weighting factor in accordance to the following ratio:

$$\alpha_i = \frac{K_{min}}{K_{Bati}} \tag{12}$$

In this way, the power sharing is proportional to the capacity of the ESSs. The Pseudo-code 1 summarizes the SoC equalization program and the assignment of the weighting factors for the microgrid considered as case study ($n = 2$).

B. Active Power Curtailment of RESs

It is expected to obtain from RESs the maximum amount of available energy. Due to their unpredictable behaviour, maximum power point tracking (MPPT) algorithms are used for ensuring the operation of PV and WT generators on their point of maximum generation ($P_{MPPT}(RESi)$). MPPT strategies are not considered in this paper, interested readers may refer to [34], [35].

When there is surplus of power generation compared to power consumption in the islanded microgrid, the ESSs can get fully charged ($SoC_{Bati} \geq SoC_{max}$). At this point, for preventing further battery charge, it is required that $P_{Bati} = 0$. Then, the power generation from RESs has to be curtailed [17], [36] while the power balance in the system should be ensured.

$$\sum_{i=1}^{n} P_{RESi} - P_{load} = 0 \tag{13}$$

To do that, the power reference (P^*), normally derived from the MPPT system, will be weighted by a curtailment index (β_i) where, ($0 \leq \beta \leq 1$). Then, in steady state:

$$P_{RESi} \approx P^* = \beta_i P_{MPPT}(RESi) \tag{14}$$

In the case of distributed RESs, the question is how much energy should be generated from each RES. In the proposed control architecture, the power contribution of each RES

Pseudo-code 1 Equalization Program

function F($K_{Bati}, P_{RESi}, P_{load}, SoC_{Bati}, Sign(P_{Bati})$)
  $K_{max} = max(K_{Bat1}, K_{Bat2})$;
  $[K_{min}, index] = min(K_{Bat1}, K_{Bat2})$;
  if $SoC_{bat1} \neq SoC_{bat1}$ **then**
    $A = [-K_{Bat1}, -K_{Bat2}; \Delta t, -\Delta t]$
    $B = [-(P_{RES1} + P_{RES2} - P_{load}); (SoC_{Bat2} - SoC_{Bat1})]$
    Solve $X = A^{-1} \times B$;
    if $Sign(P_{Bat1})$ **and** $Sign(P_{Bat2}) = 1$ **then**
      if $SoC_{Bat1} > SoC_{Bat2}$ **then**
        $\alpha_2 = (K_{min}/K_{max})$;
        $\alpha_1 = \alpha_2(K_{Bat2} \cdot X(2))/(K_{Bat1} \cdot X(1))$
      else
        $\alpha_1 = (K_{min}/K_{max})$;
        $\alpha_2 = \alpha_1(K_{Bat1} \cdot X(1))/(K_{Bat2} \cdot X(2))$
      end if
    else
      if $SoC_{Bat1} > SoC_{Bat2}$ **then**
        $\alpha_1 = (K_{min}/K_{max})$;
        $\alpha_2 = \alpha_1(K_{Bat1} \cdot X(1))/(K_{Bat2} \cdot X(2))$
      else
        $\alpha_2 = (K_{min}/K_{max})$;
        $\alpha_1 = \alpha_2(K_{Bat2} \cdot X(2))/(K_{Bat1} \cdot X(1))$
      end if
    end if
    return α_1, α_2
    Wait for Δt
  else
    switch $index$ **do**
      case 1
        $\alpha_1 = 1$;
        $\alpha_2 = (K_{min}/K_{Bat2})$;
      case 2
        $\alpha_1 = (K_{min}/K_{Bat1})$;
        $\alpha_2 = 1$;
  end if
end function

(P_{RESi}) will be proportional to its maximum available Power ($P_{MPPT}(RESi)$). Then:

$$\frac{P_{RES1}}{P_{RES2}} = \frac{\beta_1}{\beta_2} \tag{15}$$

The Pseudo-code 2 summarizes the program for determining the curtailment indexes (β_i) for the case study microgrid ($n = 2$). The program basically solves the linear system composed of equations (13) and (15). This program will be activated once the SoC of any of the distributed ESSs reaches the threshold value (SoC_{max}) and will be maintained provided that the maximum available power is greater than the power consumption ($P_{MPPT}(RES1) + P_{MPPT}(RES2) > P_{load}$).

C. Load Shedding

Over-discharge of ESSs based on batteries may not only affect the performance of the batteries but also affects the stability of the islanded microgrid. Below certain voltage value, the stored energy of the batteries can be considered as completely delivered, and the voltage would drop quickly if the discharge continues. This fact may affect the regulation of the microgrid because the voltage of the batteries will approach rapidly to zero. Because of that, over-discharge of batteries

Pseudo-code 2 Curtailment Index

function F($P_{MPPT}(RES1), P_{MPPT}(RES2), P_{load}$)
  if ($SoC_{Bat1} \geq SoC_{max} \parallel SoC_{Bat2} \geq SoC_{max}$) **then**
    do
      $A1 = [P_{MPPT}(RES1), P_{MPPT}(RES2); P_{MPPT}(RES2), -P_{MPPT}(RES1)]$;
      $B1 = [P_{load}; 0]$;
      Solve $X1 = A1^{-1} \times B1$;
      $\beta_1 = X1(1)$;
      $\beta_2 = X1(2)$;
    while $P_{MPPT}(RES1) + P_{MPPT}(RES2) > P_{load}$
  else
    $\beta_1 = 1$;
    $\beta_2 = 1$;
  end if
end function

should be avoided once the batteries reach a cut-off value commonly known as the end of discharge (EOD) voltage. This value corresponds roughly to 20% of the SoC and is typically specified by the battery manufacturers [4], [37].

Since, in the case study microgrid, there is not a dispatchable generator for supplying the load and charging the battery at the same time, it is required to cut-off the load for keeping a safe window for the SoC. Once any of the distributed ESSs has reached the EOD voltage $V_{Bati} \leq EOD(V)$, the MGCC should send a command to the load control and metering unit for disconnecting the load $x_{LOAD} = 0$.

When the load is disconnected, the ESSs will be charged in accordance to the available energy from RESs. For the proposed control architecture, it is considered a reconnection of the load once the SoC in both ESSs is greater than 60% ($x_{LOAD} = 1$). The Pseudo-code 3 summarizes the program for load-shedding.

Pseudo-code 3 Load-shedding

function F(SoC_{Bati}, V_{Bati})
  if ($V_{bat1} \leq EOD \parallel V_{bat2} \leq EOD$) **then**
    do
      $x_{LOAD} = 0$;
    while $SoC_{Bat1} \leq 60$ & $SoC_{Bat1} \leq 60$
  else
    $x_{LOAD} = 1$;
  end if
end function

IV. Case Study Microgrid

Table I summarizes the main parameters of the case study islanded ac microgrid which is composed of two RESs, two ESSs and a resistive aggregated load as shown in Fig. 1.

A. Experimental Setup

The experimental setup can be divided into four part as can be seen in Fig. 5.

1) MGCC: It has been deployed by using LabVIEW in a central computer. The LabView platform contains all the supervisory tasks performed by the MGCC explained in the previous section.

TABLE I: Parameters of the Microgrid

Parameter	Symbol	Value
Power Stage		
Nominal Bus Voltage	E^*	$230 * \sqrt{2}$ V
Nominal Bus Frequency	f^*	50 Hz
Inverter inductors	$L1, L2$	1.8 mH
Filter Capacitor	C	27μF
ESSs Parameters		
Nominal Voltage	$VBat$	720 V
End-of-discharge voltage	EOD	685 V
Maximum SoC	SoC_{max}	90 %
Minimum SoC	SoC_{min}	30 %
Battery Capacity	C_{bat}	10 Ah
Maximum power for ESSs	P_{max}	2000 W
Equalization time	Δt	30 min
Power flow Control		
Droop Coefficient $(P-\omega)$	K_p	$1.2 * 10^{-5}$ rad/s/W
Droop Coefficient $(Q-E)$	K_q	$5 * 10^{-4}$ V/VAr
Reactive power reference	Q^*	0 VAr

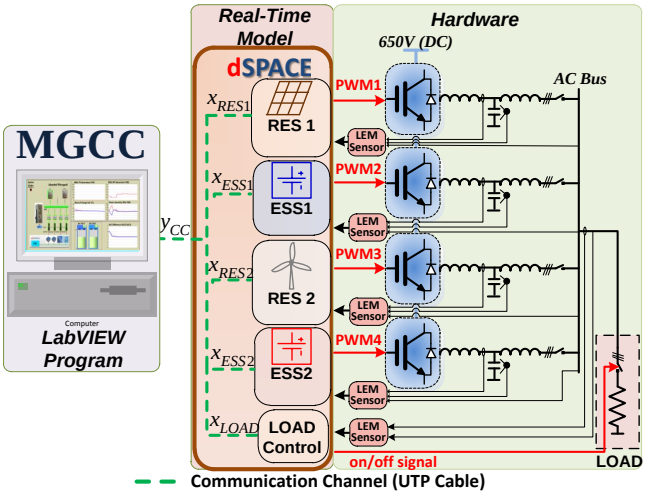

Fig. 5: Experimental setup configuration.

2) Hardware part: It is composed of four inverters Danfoss (2.2 kW), LCL filters and measurement sensors. Fig. 6 shows an image of the experimental setup. All the inverters are supplied by a stiff dc bus of 650V which emulates the intermediate dc-link between the grid-side inverter and the energy source.

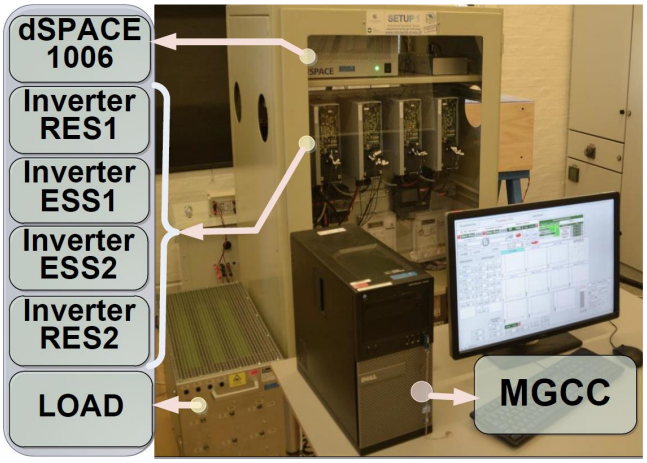

Fig. 6: Image of the Experimental Setup.

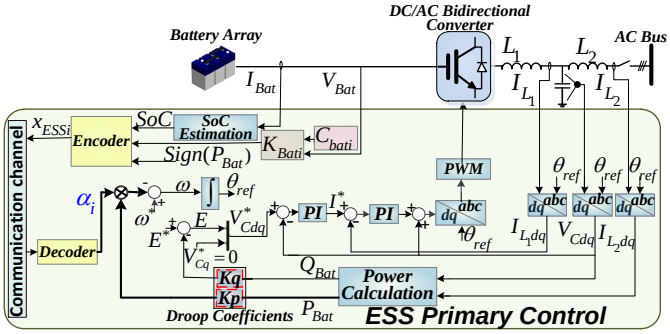

Fig. 7: Scheme of the primary control for ESSs.

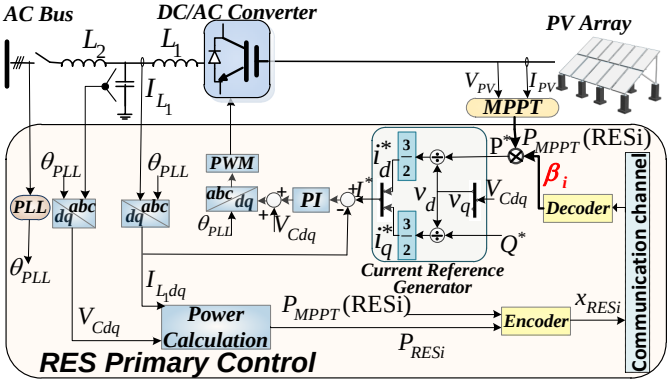

Fig. 8: Scheme of the primary control for RESs.

3) Real-Time simulation part: It is implemented in a dSPACE1006 control board which contains detailed models of the batteries, as proposed in [38], for emulating their slow and fast dynamics. RESs are emulated as constant power generators. Then, the control board contains the generation profiles of RESs. On top of that, the Real-Time control board contains the primary controllers and generates the control signals for each inverter.

Fig. 7 shows the scheme of the primary control for ESSs which is composed of an inner current control loop, outer voltage control loop, the droop control loop, which is adjusted by the signal α_i, and the encoder/decoder units for linking the ESS with the communication channel. Similarly, Figs. 8 shows the scheme of the primary control for RESs. The reference of the inner current control loop is determined by the MPPT algorithm, which is weighted by the parameter β_i.

4) Communication channel: It is a wired full-duplex communication channel, where the User Datagram Protocol (UDP) is used for interchanging data between each distributed energy unit and the MGCC. The data set sent from each RES (X_{RESi}), each ESS (X_{ESSi}), and the load (X_{LOAD}) are:

$$X_{RESi} = [P_{RESi}, P_{MPPT}(RESi)]^T \quad (16)$$

$$X_{ESSi} = [K_{Bati}, SoC_{Bati}, Sign(P_{Bati})]^T \quad (17)$$

$$X_{LOAD} = [P_{load}]^T \quad (18)$$

Meanwhile, the data set sent from the MGCC to the distributed units y_{CC}, is defined as:

$$y_{CC} = \begin{cases} [\alpha_i]^T, & \textbf{for } ESSi; \\ [\beta_i]]^T, & \textbf{for } RESi; \\ [x_{LOAD}], & \textbf{for } LOAD. \end{cases} \quad (19)$$

The effect of communication delay has not been considered in this paper. Possible delays in the communication are mainly due to the processing performed by the protocol and the execution time of the programs, while the propagation delay can be neglected in this kind of wired LAN applications [39], [40]. The estimated maximum latency of a simple LAN Ethernet network is up to $1.85\,ms$, under full-size frame of 1518 bytes [41]. In addition, the maximum execution time of the programs in the MGCC is around $150\,ms$. Previous works have analysed the impact of communication delay for an islanded microgrid communicated with a central secondary control where the microgrid is able to keep good performance for communication delays up to $200ms$ [42]. On top of that, by considering fast dynamic response of the primary controllers, the dynamic interaction of the microgrid with the MGCC depends mainly on the times for charging or discharging the batteries (seconds, minutes or hours depending on the battery capacity). Therefore, it is still acceptable to neglect the time delay.

B. Stability Considerations

Since the droop control loops will be adjusted for the equalization of the SoCs, it is important to evaluate the dynamic performance of the microgrid operating as shown in Fig. 2, with both ESSs as master units, with adaptive droop coefficients. The stability analysis and dynamic models are completely explained in [31], where stable dynamic response with minimum damping is ensured by selecting the nominal values of the droop coefficients (K_p and K_q). Interested readers may refer to [31] for deeper explanation about the small-signal model.

However, the equalization program in (Pseudo-code 1) may generate negative values of the weighting factors α_i after solving the linear equation system in the program. In this case, the dynamic response of the microgrid will be unstable as shown in Fig. 9, where α_1 is kept at 1 (the droop coefficient of ESS1 is kept on its nominal value) and α_2 changes between -1 to 1 (the droop coefficient of ESS2 is adjusted). Fig. 9 shows that the system is stable for positive values of the weighting factors and unstable for negative values. In light of the above, the weighting factors should be limited to zero in the lower limit to avoid negative values. This fact may cause that more than one iterations are required before reaching the equalization but the stability of the microgrid is ensured.

C. Selection of the Equalization Time Δt

The minimum time for executing the equalization program (Δt_{min}) is restricted by the maximum power that each ESS can manage (P_{max}) in accordance to:

$$\Delta t_{min} = -\frac{\Delta SoC_{max}}{P_{max}} K_{nom} \tag{20}$$

where, ΔSoC_{max} is the maximum variation in the SoC during equalization, K_{nom} is calculated with the largest capacity value among the distributed ESS units in the microgrid and the nominal voltage of the battery array as shown in equation (5). The equalization time can be selected with any value larger than (Δt_{min}). However, it is advisable to select the equalization time (Δt) closer to (Δt_{min}), for faster equalization. In this case study, it is considered a maximum variation of SoC $(\Delta SoC_{max} = 10\%)$ and $(\Delta t = 30\,min)$.

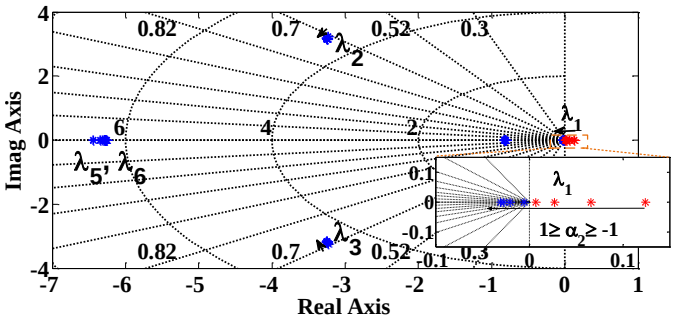

Fig. 9: Root locus plot of the microgrid under adjustment of weighting factors α_i.

V. Results

In order to speed-up the implementation time, the experiments have been scaled in the time base of 1 hour to 20 seconds ($3600s \rightarrow 20s$). Therefore, a time horizon of 24 hours corresponds to 480 seconds. Accordingly, the real capacity of the battery, C_{bat}, is scaled for the experiment by applying the simple relation,

$$C_{bati}(expe) = C_{bati}(Ah) * \frac{20s}{3600s} \tag{21}$$

Initially, two experiments has been performed in order to evaluate the operation of the microgrid with the MGCC under different operational conditions of the microgrid.

A. First Experiment

The first experiment considers surplus of energy generation in a time horizon of 24 hours, for a constant load consumption of $690\,W$. Additionally, the experiment considers different battery capacities for each ESS; ($C_{Bat1} = 5\,A \cdot h$ for ESS1 and $C_{Bat2} = 10\,A \cdot h$), and different initial SoC in each ESS ($SoC_{Bat1} = 70\,\%$ and $SoC_{Bat2} = 80\,\%$). Fig. 10 shows: (a) the SoCs, (b) the error value, defined as $(Error = SoC_{Bat2} - SoC_{Bat1})$, (c) the battery voltages in both ESSs, (d) the power shared between distributed ESSs, (e) and (f) show the power generation profiles (P_{RESi}) and the maximum power available for each RESs $(P_{MPPT}(RESi))$ for RES1 and RES2 respectively. For an easy explanation, Fig. 10 is divided into four time slots (S1 to S4) as follows:

S1 (t_0-t_1): The ESSs are discharged while the equalization program reduces the $Error$ and equalizes the SoCs by adjusting the active power shared by the ESSs. It is possible to see that at least two iterations of the equalization program are required to reach $Error = 0$. In general, the additional iterations in the equalization process are due to three main reasons: 1) the equalization program is based on linear models which do not consider dynamic and transient responses of the microgrid. This fact causes mismatches between the expected behaviour shown in Fig. 3 and the real dynamic behaviour, 2) the consumption and generation were assumed

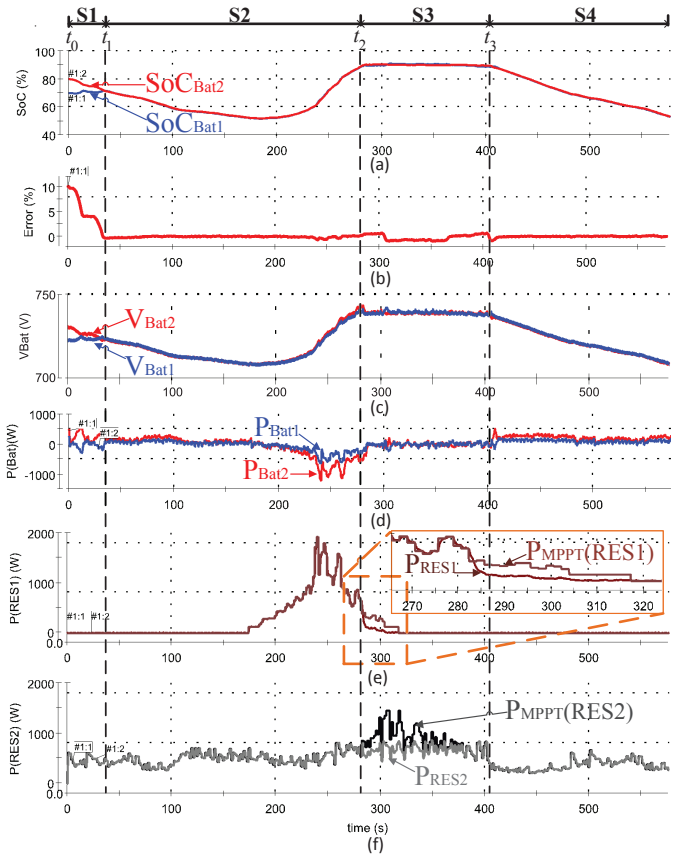

Fig. 10: Experimental results considering surplus in power generation.

as constant during the equalization time. However, due to the unpredictable behaviour of RESs or even changes in the load consumption, the conditions for equalization are not held during the equalization time, 3) as mentioned in section IV. *B.*, the lowest value in the weighting factors is limited to zero. Despite the aforementioned conditions, the equalization can be achieved within few iterations.

S2 (t_1-t_2): During this stage, the ESSs are discharged and charged while keeping the power balance in the microgrid. In Fig. 10(d), it is possible to see how the power shared by each ESS is proportional to its battery capacity in order to keep equalized the SoCs ($|P_{Bat2}| \geq |P_{Bat1}|$).

It is possible to see from t_1 that the equalization program keeps equalized the SoCs and ensures equal SoC profiles for the distributed ESSs. This response emulates the behaviour that would have a single aggregate energy storage unit. In the end, this is reflected in uniform conditions of degradation and cycle for the distributed ESSs. Also, this fact allows an easy definition of unified coordinated actions in the microgrid, which ensure operation of the distributed ESSs within a safe operation window for the SoCs.

S3 (t_2-t_3): At t_2, the SoCs in the ESSs reach the SoC_{max} value. As a consequence, the active power curtailment program is activated and the power generation from RESs is adjusted proportionally to their own maximum available power. This behaviour keeps the power balance in the microgrid and avoids overcharge of the ESSs. Additionally, it is possible to see how

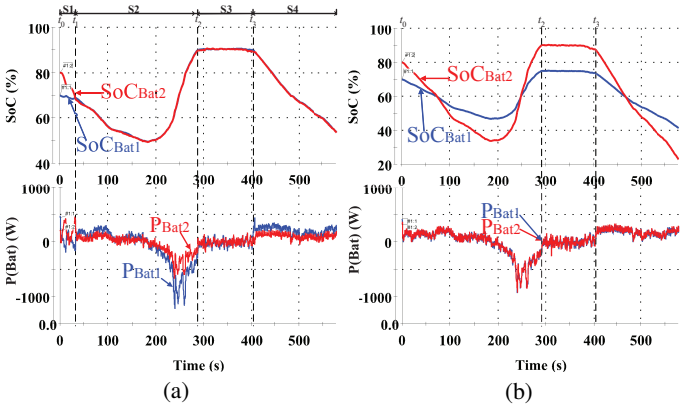

Fig. 11: SoC and power sharing profiles: (a) with the equalization program, (b) without equalization.

the equalization program manages to reduce any difference that may appear between SoCs.

S4 (t_3-): The power generation from RESs is not enough to keep the power balance in the microgrid, then the ESSs re-assume this responsibility and are discharged accordingly.

Fig. 11 shows the SoC and power sharing profiles obtained experimentally with and without the proposed equalization program. In this case, the capacity values have been exchanged in comparison with the previous case ($C_{Bat1} = 10\,A \cdot h$ for ESS1 and $C_{Bat2} = 5\,A \cdot h$), but the initial SoC values and profiles of consumption and generation are equal. In Fig. 11(a) is shown that uniform SoC profiles are achieved even with different values in the capacities. Also, it is possible to see that the SoC profiles in Figs. 10(a) and 11(a) are pretty similar, since the total capacity of the batteries is equal in both cases ($C_{total} = C_{Bat1} + C_{Bat2} = 15\,A \cdot h$). In particular, this would be the behaviour of an aggregated ESS of $15\,A \cdot h$ without the equalization time. Additionally, Fig. 11(a) shows that after the equalization period (S1), the power is shared proportionally to the capacity of each ESS ($|P_{Bat2}| < |P_{Bat1}|$). This behaviour in the power sharing is inverse to the behaviour observed in the previous case (Fig. 10(d)).

Fig. 11(b) shows the behaviour of the ESSs without the equalization program. Here, the power is equally shared by means of conventional droop control loops with equal values of the droop coefficients. In this case, the amplitude of the cycle and the depth of discharge (DoD(%)=100-SoC(%)) are larger for ESS2 than for ESS1. Because of this, ESS2 will be exposed to more degradation compared to ESS1. Additionally, the overall degradation of the ESSs would be larger without the use of the equalization program, since larger DoD values are reached without the equalization ($DoD \approx 80\,\%$ in Fig. 11(b) compared with $DoD \approx 50\,\%$ in Fig. 11(a)).

B. Second Experiment

The second experiment considers more demand than generation in a time horizon of 24 hours. For this case, the constant load consumption is increased to $1333\,W$ with the same generation used in the previous experiment. Apart from that, this experiment considers the same battery capacity for both ESSs ($C_{Bat1} = C_{Bat2} = 10\,A \cdot h$). The initial SoCs are set to 75 % for ESS1 and 85 % for ESS2. Fig. 12 shows:

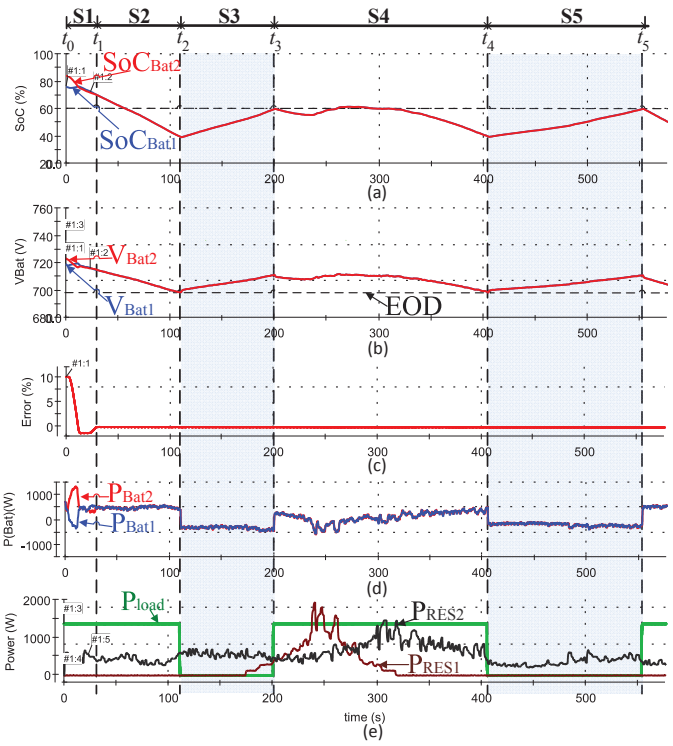

Fig. 12: Experiment results considering more consumption than generation.

(a) the SoCs, (b) the battery voltages in both ESSs, (c) the error value, (d) the power shared between distributed ESSs, and (e) the power generation profiles (P_{RESi}) and the load consumption (P_{load}).

S1 (t_0-t_1): The SoCs are equalized by adjusting the active power shared by the ESSs. Here, it is also possible to see that the equalization is achieved after more than one iteration of the equalization program.

S2 (t_1-t_2): The ESSs are discharged with the SoCs completely equalized ($Error = 0$). The active power is shared equally between the two ESSs because they have the same battery capacity. At t_2, the battery voltages drop until the EOD value.

S3 (t_2-t_3): During this stage the load is disconnected in order to prevent further discharge of the ESSs. The ESSs are charged with all the energy available from the renewable generation until the SoCs of ESSs reach the 60 % in t_3.

S4 (t_3-t_4): The load is connected in t_3 and the ESSs are discharged and charged for keeping the power balance in the microgrid. At t_4 the battery voltages reach again the EOD value.

S5 (t_4-t_5): The process is similar to S3, the load is disconnected in t_4 and connected again in t_5.

C. Optimized Load Disconnection

From Fig. 12(e) it is possible to see that the load can have many connection/disconnection cycles during a day, due to the intermittent nature of RESs generation. Despite the fact that the disconnection of the load is inevitable under certain operational conditions, intermittent connection and disconnection cycles are not the best option for loads which need continuous supply for performing specific task. To solve this problem, the load can be shifted to be connected within specific time slots in which continuous energy supply can be ensured by the microgrid. In this sense, an optimization model is used to schedule the load disconnection in order to minimize the number of reconnection.

This optimization has been developed as a mixed integer linear programming problem for a time horizon of $T = 24$ hours. The index $h = 1, 2, \ldots, H$, is defined as the elementary discrete times of the forecasted data where ($H = \frac{T}{\Delta h} = 24$). The optimization problem is tested by using data of generation and consumption assuming 24-h ahead forecasted data, with time slots of one hour ($\Delta h = 1$). The optimization problem minimizes the objective function,

$$\min_{\bar{x}} \sum_{h=1}^{H} \xi_1 * P_{load}\Delta h * (1 - z_L(h)) + \sum_{h=1}^{H} \xi_2 * P_{load}\Delta h * z_{start}(h) + \sum_{h=1}^{H} \xi_3 * P_{excess}(h)\Delta h \quad (22)$$

in terms of the set of variables defined as,

$$\bar{x} = \begin{pmatrix} z_L(h) \\ z_{start}(h) \\ P_{Bati}(h) \\ SoC_{(Bati)}(h) \\ P_{excess}(h) \end{pmatrix} \quad (23)$$

where, $z_L(h)$ and $z_{start}(h)$ are binary variables related to the load ($z_L(h), z_{start}(h) \in \{0,1\}, \forall h$), and $P_{excess}(h)$ represents the surplus of RESs generation that may be curtailed within the operation of the islanded microgrid. Here, the powers and SoCs are considered as average values for every time slot. Particularly, $z_L(h)$ defines the status of the load and it is equal to zero if the load is disconnected, and, $z_{start}(h)$ is an auxiliary variable to identify when the load has been connected. In (22), ξ_1, ξ_2 and ξ_3 are cost coefficients with $\xi_1 \geq \xi_2 > \xi_3$, in order to prioritize the connection of the load over the storage of the surplus energy.

The first term in (22) corresponds to the penalization for disconnecting the load and will be zero if the load is connected. The second term is the penalization for reconnecting the load. In this way, the optimization problem will minimize the number of reconnection and the load will be kept connected for longer periods. The third term penalizes the curtailment of RESs generation.

Furthermore, the model contains a set of constraints that makes the problem feasible. To start with, the energy balance should be fulfilled. This fact can be written as,

$$\sum_{i=1}^{n} P_{MPPT}(RESi)(h)\Delta h + \sum_{k=1}^{n_k} P_{Bati}(h)\Delta h = P_{load}\Delta h * z_L(h) + P_{excess}(h)\Delta h, \quad \forall h \quad (24)$$

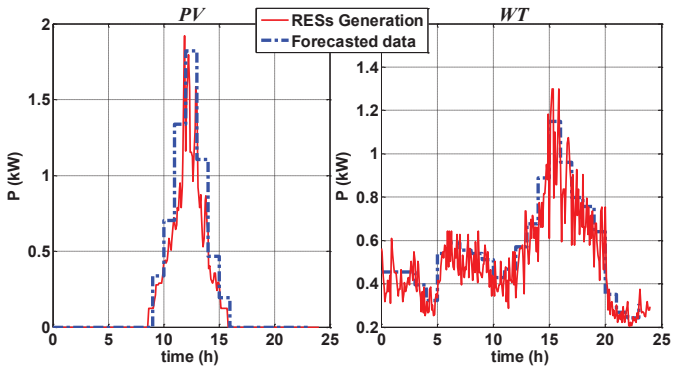

Fig. 13: Comparison: Forecasted Data and RESs Generation Profiles.

where, $P_{MPPT}(RESi)(h)\Delta h$ is the energy provided by the i-th RES. The variables in (24) are bounded as,

$$0 \leq P_{excess}(h) \leq \sum_{i=1}^{n} P_{MPPT}(RESi)(h), \quad \forall h \tag{25}$$

$$-P_{max} \leq P_{Bati}(h) \leq P_{max}, \quad \forall h, i \tag{26}$$

In order to use the variable $z_{start}(h)$, the following condition should be established,

$$z_{start}(h) \geq z_L(h) - z_L(h-1), \quad \forall h \tag{27}$$

In this way, $z_{start}(h)$ is set to 1 when $z_L(h)$ changes from 0 to 1, and the optimization problem determines the rest of values in order to minimize the number of intermittent cycles in the load.

Regarding the ESSs, the SoCs can be estimated as a function of its previous value and the current power as,

$$SoC_{Bati}(h) = SoC_{Bati}(h-1) - \frac{\eta_{Bati}}{C_{Bati}} P_{Bati}(h)\Delta h, \quad \forall h, i \tag{28}$$

The SoC is limited in the range,

$$SoC_{min} \leq SoC_{Bati}(h) \leq SoC_{max}, \quad \forall h, i \tag{29}$$

And finally, the effect of the equalization is approximated as,

$$SoC_{Bat1}(h) = SoC_{(Bat2)}(h), \quad \forall h \geq 1, i \geq 2 \tag{30}$$

In this way, the ESSs are supposed to be equalized after the first time slot (1 hour), but it can be changed for instance to the second time slot by setting $\forall h \geq 2$.

The operation of the MGCC is complemented with the optimal scheduling for the load connection. However, due to probable mismatches between the forecasted data and RESs generation, as can be seen in Fig. 13, the connection of the load is determined by the conjunction of the status signals (x_{LOAD} & z_L) in order to avoid any operation beyond specified operation limits for the ESSs.

Fig. 14 shows the operation of the microgrid complemented with the optimal scheduling of the load connection. In addition to the SoCs profiles, the voltages of the batteries, and the RESs generation and load profiles (Figs. 14(a), (b) and (c) respectively), Fig. 14(d) shows the status signals for enabling

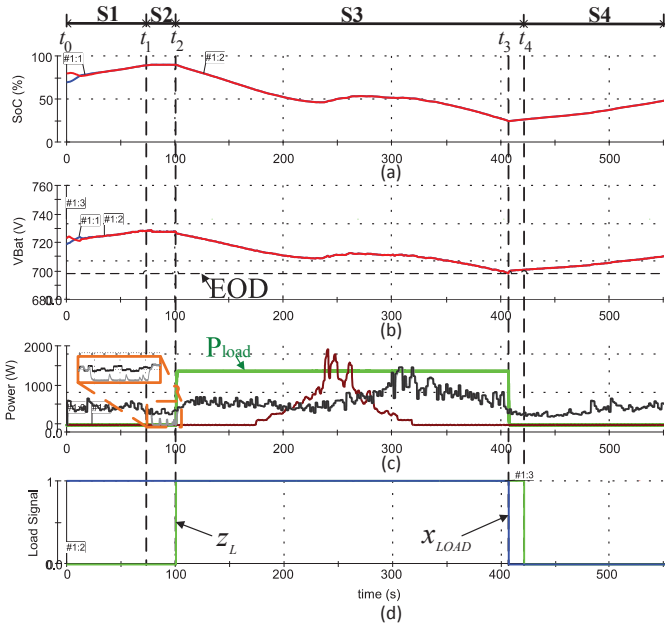

Fig. 14: Experiment results with optimized load connection.

the connection or disconnection of the load (x_{LOAD} and z_L). It is possible to see that the load connection/disconnection cycles are reduced during a day and continuous periods for supplying energy to the load are ensured.

S1 (t_0-t_1): The load is scheduled to be disconnected ($z_L = 0$) and the ESSs are charged by the available RESs generation.

S2 (t_1-t_2): The SoCs reach the SoC_{max} value. Then, the active power curtailment program is activated and the power generation from RES2 is reduced.

S3 (t_2-t_3): The load is scheduled to be connected ($z_L = 1$) and the ESSs compensate any mismatch between generation and consumption. At t_3 the battery voltages reach the EOD value ($x_{LOAD} = 0$).

S3 (t_3-t_4): The load is disconnected for preventing any discharge of the ESSs beyond safe operating limits, even if the load connection is still scheduled ($x_{LOAD} = 0$ & z_L=1). This period shows the behaviour by considering mismatches between prediction and real operation. As can be seen, safe operation limits are still ensured.

S4 (t_4-): The load is scheduled to be disconnected ($z_L = 0$) by the optimization program.

VI. Conclusion

This paper proposes a centralized coordination strategy for small-scale islanded microgrids based on distributed energy generation and distributed energy storage systems. The coordination strategy includes an effective method for equalizing the state of charge, even for distributed ESSs with different capacities. The equalization function looks for uniform cycle profiles and similar degradation of the distributed ESSs. Because of this, the distributed ESSs can be seen as an aggregated ESSs from the point of view of the coordination strategy. This fact facilitates the definition of simple coordinated actions, such as power curtailment and load shedding, since the threshold levels for a safe operation of the distributed ESSs are reached

almost at the same time in all the distributed storage units. The proposed strategy is ideal for the integration of distributed active generators (RESs+ESS), in which the ESS has been sized optimally for smoothing the variable nature of a specific RES. Additionally, the strategy is complemented with an optimization program which ensures a continuous supply of energy to the load. As a result, the load can be shifted accordingly for performing specific actions within specific periods. Stable and reliable operations are considered and ensured for the islanded microgrid and the strategy was tested experimentally. The proposed strategy can be easily scaled for microgrids with more distributed energy resources and loads.

REFERENCES

[1] H. Beltran, E. Bilbao, E. Belenguer, I. Etxeberria-Otadui, and P. Rodriguez, "Evaluation of storage energy requirements for constant production in pv power plants," *IEEE Transactions on Industrial Electronics*, vol. 60, pp. 1225–1234, March 2013.

[2] J. Y. Kim, J. H. Jeon, S. K. Kim, C. Cho, J. H. Park, H. M. Kim, and K. Y. Nam, "Cooperative control strategy of energy storage system and microsources for stabilizing the microgrid during islanded operation," *IEEE Transactions on Power Electronics*, vol. 25, pp. 3037–3048, Dec 2010.

[3] D. Wu, F. Tang, T. Dragičević, J. Vasquez, and J. Guerrero, "A control architecture to coordinate renewable energy sources and energy storage systems in islanded microgrids," *IEEE Transactions on Smart Grid*, vol. 6, pp. 1156–1166, May 2015.

[4] F. Marra and G. Yang, "Chapter 10 - decentralized energy storage in residential feeders with photovoltaics," in *Energy Storage for Smart Grids* (P. D. Lu, ed.), pp. 277 – 294, Boston: Academic Press, 2015.

[5] H. Mahmood, D. Michaelson, and J. Jiang, "Strategies for independent deployment and autonomous control of pv and battery units in islanded microgrids," *IEEE Journal of Emerging and Selected Topics in Power Electronics*, vol. 3, pp. 742–755, Sept 2015.

[6] J. de Matos, F. S.F.e Silva, and L. de S Ribeiro, "Power control in ac isolated microgrids with renewable energy sources and energy storage systems," *IEEE Transactions on Industrial Electronics*, vol. 62, pp. 3490–3498, June 2015.

[7] E. Liegmann and R. Majumder, "An efficient method of multiple storage control in microgrids," *IEEE Transactions on Power Systems*, vol. 30, pp. 3437–3444, Nov 2015.

[8] W. Huang and J. Abu Qahouq, "Energy sharing control scheme for state-of-charge balancing of distributed battery energy storage system," *IEEE Transactions on Industrial Electronics*, vol. 62, pp. 2764–2776, May 2015.

[9] X. Lu, K. Sun, J. Guerrero, J. Vasquez, and L. Huang, "State-of-charge balance using adaptive droop control for distributed energy storage systems in dc microgrid applications," *IEEE Transactions on Industrial Electronics*, vol. 61, pp. 2804–2815, June 2014.

[10] X. Lu, K. Sun, J. Guerrero, J. Vasquez, and L. Huang, "Double-quadrant state-of-charge-based droop control method for distributed energy storage systems in autonomous dc microgrids," *IEEE Transactions on Smart Grid*, vol. 6, pp. 147–157, Jan 2015.

[11] N. L. Díaz, T. Dragičević, J. C. Vasquez, and J. M. Guerrero, "Intelligent distributed generation and storage units for dc microgrids - a new concept on cooperative control without communications beyond droop control," *IEEE Transactions on Smart Grid*, vol. 5, pp. 2476–2485, Sept 2014.

[12] T. R. Oliveira, W. W. A. G. Silva, and P. F. Donoso-Garcia, "Distributed secondary level control for energy storage management in dc microgrids," *IEEE Transactions on Smart Grid*, vol. PP, no. 99, pp. 1–11, 2016.

[13] T. Dragičević, J. M. Guerrero, J. C. Vasquez, and D. Škrlec, "Supervisory control of an adaptive-droop regulated dc microgrid with battery management capability," *IEEE Transactions on Power Electronics*, vol. 29, pp. 695–706, Feb 2014.

[14] Q. Shafiee, T. Dragičević, J. C. Vasquez, and J. M. Guerrero, "Hierarchical control for multiple dc-microgrids clusters," *IEEE Transactions on Energy Conversion*, vol. 29, pp. 922–933, Dec 2014.

[15] N. L. Diaz, A. C. Luna, J. C. Vasquez, and J. M. Guerrero, "Equalization algorithm for distributed energy storage systems in islanded ac microgrids," in *41st Annual Conference of the IEEE Industrial Electronics Society, IECON 2015*, pp. 004661–004666, Nov 2015.

[16] J. Guerrero, J. Vasquez, J. Matas, L. de Vicuña, and M. Castilla, "Hierarchical control of droop-controlled ac and dc microgrids;a general approach toward standardization," *IEEE Transactions on Industrial Electronics*, vol. 58, pp. 158–172, Jan 2011.

[17] M. Mao, H. Huang, and L. Chang, "Real-time energy coordinated and balance control strategies for microgrid with photovoltaic generators," in *Power Electronics for Distributed Generation Systems (PEDG), 2013 4th IEEE International Symposium on*, pp. 1–7, July 2013.

[18] Z. Guo, D. Sha, and X. Liao, "Energy management by using point of common coupling frequency as an agent for islanded microgrids," *IET Power Electronics*, vol. 7, pp. 2111–2122, August 2014.

[19] N. Diaz, D. Wu, T. Dragicevic, J. Vasquez, and J. Guerrero, "Fuzzy droop control loops adjustment for stored energy balance in distributed energy storage system," in *2015 9th International Conference on Power Electronics and ECCE Asia (ICPE-ECCE Asia)*, pp. 728–735, June 2015.

[20] F. Katiraei, R. Iravani, N. Hatziargyriou, and A. Dimeas, "Microgrids management," *IEEE Power and Energy Magazine*, vol. 6, pp. 54–65, May 2008.

[21] W. Shi, X. Xie, C.-C. Chu, and R. Gadh, "Distributed optimal energy management in microgrids," *IEEE Transactions on Smart Grid*, vol. 6, pp. 1137–1146, May 2015.

[22] B. Wang, M. Sechilariu, and F. Locment, "Intelligent dc microgrid with smart grid communications: Control strategy consideration and design," *IEEE Transactions on Smart Grid*, vol. 3, pp. 2148–2156, Dec 2012.

[23] D. Wu, F. Tang, T. Dragicevic, J. Vasquez, and J. Guerrero, "Autonomous active power control for islanded ac microgrids with photovoltaic generation and energy storage system," *IEEE Transactions on Energy Conversion*, vol. 29, pp. 882–892, Dec 2014.

[24] O. de Sousa-Perez, J. Miret, A. Camacho, P. Marti, and R. Guzman, "Power sharing control in islanded microgrid using event driven communication," in *39th Annual Conference of the IEEE Industrial Electronics Society, IECON 2013*, pp. 2151–2156, Nov 2013.

[25] J. Pecas Lopes, C. Moreira, and A. Madureira, "Defining control strategies for microgrids islanded operation," *IEEE Transactions on Power Systems*, vol. 21, pp. 916–924, May 2006.

[26] A. Kahrobaeian and Y. A. R. I. Mohamed, "Networked-based hybrid distributed power sharing and control for islanded microgrid systems," *IEEE Transactions on Power Electronics*, vol. 30, pp. 603–617, Feb 2015.

[27] N. L. Díaz, J. G. Guarnizo, M. Mellado, J. C. Vasquez, and J. M. Guerrero, "A robot-soccer-coordination inspired control architecture applied to islanded microgrids," *IEEE Transactions on Power Electronics*, vol. PP, no. 99, pp. 1–1, 2016.

[28] L. Meng, X. Zhao, F. Tang, M. Savaghebi, T. Dragicevic, J. Vasquez, and J. Guerrero, "Distributed voltage unbalance compensation in islanded microgrids by using a dynamic consensus algorithm," *IEEE Transactions on Power Electronics*, vol. 31, pp. 827–838, Jan 2016.

[29] L. Siow, P. So, H. Gooi, F. Luo, C. Gajanayake, and Q. Vo, "Wi-fi based server in microgrid energy management system," in *IEEE Region 10 Conference TENCON 2009*, pp. 1–5, Jan 2009.

[30] A. Llaria, O. Curea, J. Jimenez, J. Martin, and A. Zuloaga, "Wireless communication system for microgrids management in islanding," in *Proceedings of the 2011-14th European Conference on Power Electronics and Applications (EPE 2011)*, pp. 1–10, Aug 2011.

[31] N. L. Díaz, E. A. Coelho, J. C. Vasquez, and J. M. Guerrero, "Stability analysis for isolated ac microgrids based on pv-active generators," in *2015 IEEE Energy Conversion Congress and Exposition (ECCE)*, pp. 4214–4221, Sept 2015.

[32] J. Guerrero, L. Garcia De Vicuna, J. Matas, M. Castilla, and J. Miret, "A wireless controller to enhance dynamic performance of parallel inverters in distributed generation systems," *IEEE Transactions on Power Electronics*, vol. 19, pp. 1205–1213, Sept 2004.

[33] E. A. A. Coelho, P. C. Cortizo, and P. F. D. Garcia, "Small-signal stability for parallel-connected inverters in stand-alone ac supply systems," *IEEE Transactions on Industry Applications*, vol. 38, pp. 533–542, Mar 2002.

[34] V. Salas, E. Olías, A. Barrado, and A. Lázaro, "Review of the maximum power point tracking algorithms for stand-alone photovoltaic systems," *Solar Energy Materials and Solar Cells*, vol. 90, no. 11, pp. 1555 – 1578, 2006.

[35] C. Patsios, A. Chaniotis, M. Rotas, and A. Kladas, "A comparison of maximum-power-point tracking control techniques for low-power

variable-speed wind generators," in *8th International Symposium on Advanced Electromechanical Motion Systems Electric Drives Joint Symposium, 2009. ELECTROMOTION 2009*, pp. 1–6, July 2009.
[36] S. Chalise, H. R. Atia, B. Poudel, and R. Tonkoski, "Impact of active power curtailment of wind turbines connected to residential feeders for overvoltage prevention," *IEEE Transactions on Sustainable Energy*, vol. 7, pp. 471–479, April 2016.
[37] D. Linden and T. Reddy, *Handbook of batteries*. McGraw-Hill handbooks, McGraw-Hill, 2002.
[38] T. Kim and W. Qiao, "A hybrid battery model capable of capturing dynamic circuit characteristics and nonlinear capacity effects," *IEEE Transactions on Energy Conversion*, vol. 26, pp. 1172–1180, Dec 2011.
[39] Q. Shafiee, Stefanović, T. Dragičević, P. Popovski, J. C. Vasquez, and J. M. Guerrero, "Robust networked control scheme for distributed secondary control of islanded microgrids," *IEEE Transactions on Industrial Electronics*, vol. 61, pp. 5363–5374, Oct 2014.
[40] X. Zhang, L. N. Bhuyan, and W.-C. Feng, "Anatomy of {UDP} and m-via for cluster communication," *Journal of Parallel and Distributed Computing*, vol. 65, no. 10, pp. 1290 – 1298, 2005.
[41] C. L. Siemens, "Latency on a switched ethernet network," *Application Note 8*.
[42] Q. Shafiee, J. Guerrero, and J. Vasquez, "Distributed secondary control for islanded microgrids-a novel approach," *IEEE Transactions on Power Electronics*, vol. 29, pp. 1018–1031, Feb 2014.

Nelson L. Díaz (S'09) received the B.S degree in Electronic Engineering from the Universidad Distrital F.J.C in 2008, and the M.S. degree in Industrial Automation from the Universidad Nacional de Colombia in 2011, Bogotá, Colombia. He is currently pursuing the Ph.D. degree from the Department of Energy Technology, Aalborg University, Aalborg, Denmark. He is member of the Research Laboratory of Alternative Energy Sources, Universidad Distrital F.J.C. and Microgrid Research Group, Aalborg University. His current research interests include microgrids and power converters control.

Adriana Carolina Luna (S'06) received the B.S. degree in electronic engineering in 2006 and M.S. degree in Industrial Automation in 2011, both from Universidad Nacional de Colombia. She is currently working toward the Ph.D degree in the Department of Energy Technology at Aalborg University, Aalborg, Denmark. Her research work is focused on energy management systems of microgrids, and specifically on architectures and algorithms for scheduling and optimization for operation level in microgrids.

Juan C. Vasquez (M'12-SM'14) received the B.S. degree in electronics engineering from the Autonomous University of Manizales, Manizales, Colombia, and the Ph.D. degree in automatic control, robotics, and computer vision from the Technical University of Catalonia, Barcelona, Spain, in 2004 and 2009, respectively. He was with the Autonomous University of Manizales working as a teaching assistant and the Technical University of Catalonia as a Post-Doctoral Assistant in 2005 and 2008 respectively. In 2011, he was Assistant Professor and from 2014 he is working as an Associate Professor at the Department of Energy Technology, Aalborg University, Denmark where he is the Vice Programme Leader of the Microgrids Research Program. From Feb. 2015 to April. 2015 he was a Visiting Scholar at the Center of Power Electronics Systems (CPES) at Virginia Tech. His current research interests include operation, advanced hierarchical and cooperative control, optimization and energy management applied to distributed generation in AC and DC microgrids. He has authored and co-authored more than 100 technical papers only in Microgrids in international IEEE conferences and journals. Dr. Vasquez is currently a member of the IEC System Evaluation Group SEG4 on LVDC Distribution and Safety for use in Developed and Developing Economies, the Renewable Energy Systems Technical Committee TC-RES in IEEE Industrial Electronics, PELS, IAS, and PES Societies.

Josep M. Guerrero (S'01-M'04-SM'08-FM'15) received the B.S. degree in telecommunications engineering, the M.S. degree in electronics engineering, and the Ph.D. degree in power electronics from the Technical University of Catalonia, Barcelona, in 1997, 2000 and 2003, respectively. Since 2011, he has been a Full Professor with the Department of Energy Technology, Aalborg University, Denmark, where he is responsible for the Microgrid Research Program. From 2012 he is a guest Professor at the Chinese Academy of Science and the Nanjing University of Aeronautics and Astronautics; from 2014 he is chair Professor in Shandong University; from 2015 he is a distinguished guest Professor in Hunan University; and from 2016 he is a visiting professor fellow at Aston University, UK. His research interests is oriented to different microgrid aspects, including power electronics, distributed energy-storage systems, hierarchical and cooperative control, energy management systems, smart metering and the internet of things for AC/DC microgrid clusters and islanded minigrids; recently specially focused on maritime microgrids for electrical ships, vessels, ferries and seaports. Prof. Guerrero is an Associate Editor for the IEEE TRANSACTIONS ON POWER ELECTRONICS, the IEEE TRANSACTIONS ON INDUSTRIAL ELECTRONICS, and the IEEE Industrial Electronics Magazine, and an Editor for the IEEE TRANSACTIONS on SMART GRID and IEEE TRANSACTIONS on ENERGY CONVERSION. He has been Guest Editor of the IEEE TRANSACTIONS ON POWER ELECTRONICS Special Issues: Power Electronics for Wind Energy Conversion and Power Electronics for Microgrids; the IEEE TRANSACTIONS ON INDUSTRIAL ELECTRONICS Special Sections: Uninterruptible Power Supplies systems, Renewable Energy Systems, Distributed Generation and Microgrids, and Industrial Applications and Implementation Issues of the Kalman Filter; the IEEE TRANSACTIONS on SMART GRID Special Issues: Smart DC Distribution Systems and Power Quality in Smart Grids; the IEEE TRANSACTIONS on ENERGY CONVERSION Special Issue on Energy Conversion in Next-generation Electric Ships. He was the chair of the Renewable Energy Systems Technical Committee of the IEEE Industrial Electronics Society. He received the best paper award of the IEEE Transactions on Energy Conversion for the period 2014-2015. In 2014 and 2015 he was awarded by Thomson Reuters as Highly Cited Researcher, and in 2015 he was elevated as IEEE Fellow for his contributions on "distributed power systems and microgrids".